ELSEVIER

International Journal of Solids and Structures 41 (2004) 4827–4844

INTERNATIONAL JOURNAL OF SOLIDS and STRUCTURES

www.elsevier.com/locate/ijsolstr

Effective elastic and failure properties of fiber aligned composites

V.A. Buryachenko [a,*], G.A. Schoeppner [b]

[a] University of Dayton Research Institute, Nonmetallic materials, 300 College Park, Dayton, OH 45469-0168, USA
[b] Air Force Research Laboratory, Materials and Manufacturing Directorate, AFRL/MLBC, Wright-Patterson AFB, OH 45433-7750, USA

Received 28 March 2003; received in revised form 30 January 2004
Available online 17 April 2004

Abstract

A digital image processing technique is used for measurement of centroid coordinates of fibers with forthcoming estimation of statistical parameters and functions describing the stochastic structure of laminated fiber composites. Comparative statistical analysis of the experimentally measured and numerically simulated fiber distributions are performed. We consider a linearly elastic composite medium, which consists of a homogeneous matrix containing a statistically homogeneous set of ellipsoidal inclusions. The multiparticle effective field method (MEFM) [Appl. Mech. Rev. 54 (2001) 1] based on the theory of functions of random variables and Green's functions is used to demonstrate the dependence of effective elastic moduli of fiber reinforced composites on the fiber radial distribution functions as estimated from measured experimental data as well as from the ensembles generated by the proposed method. The MEFM is applied for the estimations of second statistical moments of stresses in both the constituents and the interfaces between the matrix and fibers. These estimations are used in turn for the prediction of the effective envelope for failure initiation. The dependence of the effective failure envelope on the elastic, geometrical, and failure parameters of the constituents and the interphase matrix/fibers are analyzed.

Keywords: A. Microstructures; B. Inhomogeneous material; C. Elastic material

1. Introduction

We consider a linearly elastic composite medium which consists of a homogeneous matrix containing a statistically homogeneous set of elliptical fibers subjected to homogeneous remote loading. The prediction of the behavior of composite materials by the use of mechanical properties of the constituents and their microstructure is a primary problem of micromechanics which can ultimately lead to the estimation of stress fields in the constituents. The quantitative description of the microtopology of heterogeneous media, such as

* Corresponding author. Tel.: +1-937-439-4756; fax.: +1-937-656-7429/258-8075.
E-mail address: buryach@aol.com (V.A. Buryachenko).

0020-7683/$ - see front matter © 2004 Elsevier Ltd. All rights reserved.
doi:10.1016/j.ijsolstr.2004.02.019

fiber composite materials, is crucial in the prediction of overall mechanical and physical properties of these materials. For example, many studies have shown that both tensile ductility and fracture properties of multiphase composite materials are strongly affected by the spatial heterogeneity of the reinforcing phases (see for references e.g. Buryachenko, 2001). Even after many years of comprehensive study by extremely laborious direct measurements and empirical relations, the effect of the structure of microinhomogeneous materials and their influence on the mechanical properties of composites are not completely understood.

Since the overall properties of composite materials are sensitive to the details of the microstructure, the geometrical basis for modeling actual microstructures is needed. Digital image analysis is available for estimating descriptors of the spatial arrangement of microstructural features observed in a cross-section of materials (see e.g. Berryman, 1985). Space Dirichlet tessellations subdividing an Euclidian space into n-dimensional bounded convex polytopes (polygons in 2D case) are widely used to characterize the spatial distribution, size, and shape of a filled phase (see e.g. Ghosh and Mukhopadhyay, 1991) providing a natural and unique approach for defining a particle's neighbors and neighborhood. The Dirichlet tessellation of the two dimensional domain w yields a network of convex Voronoi polygons each containing a single inclusion with the center $\mathbf{x}_i$ $(i = 1, \ldots, n)$. The interior of the Voronoi cell associated with the point $\mathbf{x}_i$ is the region $w_i = \{\mathbf{x} \in w : |\mathbf{x} - \mathbf{x}_i| < |\mathbf{x} - \mathbf{x}_j|, \forall j \neq i\}$ that is the neighborhood of $\mathbf{x}_i$. The tessellation is constructed by plotting lines to the centers of all nearby particles and then constructing perpendicular bisecting planes to those lines. Green and Sibson (1977) have proposed the algorithm generating Voronoi polygons for n points by computing in $O(n \log n)$ time by tracing boundary adjustments, as a new polygon is fitted into a previously generated set. Ghosh et al. (1997) have developed a material based Voronoi cell method for directly treating multiple phase Voronoi polygons as elements in a finite element model for elastic and thermoelastoplastic problems. They suggested a modification to the standard tessellation procedure that protects against the situation when neighboring fibers are substantially different in size and are closely spaced, leading to polygons which do not completely envelop their corresponding fibers and may instead "cut" though the fibers. Since each Voronoi cell contains a single particle surrounded by matrix, the Dirichlet tessellation can be used for describing the statistical nature of the structure in the form of the frequency distribution of the ratio of particle-to-cell volume which is also a measure of particle clustering (see e.g. Bhattacharyya and Lagoudas, 2000).

A most common method of modeling these types of structures is to use the Monte Carlo (MC) simulation to generate a random distribution of inclusions followed by a finite element analysis (FEA) of periodically distributed mesocells containing a reasonably large number of inclusions. The usual shortcomings of the MC simulation are the prohibitive computer costs for a reasonably large number of inclusions in the mesocells. This computational cost becomes an irresistible obstacle especially for estimation of the first and second statistical moments of stresses in the constituents in the local and, especially, nonlocal problems (such estimations are absent in the case of the FEA and available for semi analytical methods (see e.g. Buryachenko, 2001; Buryachenko and Pagano, 2003; Buryachenko and Tandon, in press where the additional references can be found) that are more sensitive than the effective elastic moduli to the microstructure). The fundamental role of the statistical averages of the second moments of stress concentration factors in failure analysis is explained by the fact that both the fiber/matrix interface failure criterion and the energy release rate are quadratic functions of the local stress distributions. Because of this, the development of analytical methods is of profound importance for the practical applications.

A considerable number of analytical methods which yield the effective elastic constants and stress averages in the components are known in the linear theory of composites. Appropriate, but by no means exhaustive, references are provided in the reviews by Shermergor (1977), Christensen (1979), Willis (1981), Mura (1987), Kreher and Pompe (1989), Nemat-Nasser and Hori (1993), Kanaun and Levin (1994), Buryachenko (2001), Torquato (2002a) and Milton (2003). It appears today that variants of the effective medium method (Kröner, 1958) and the mean field method (Mori and Tanaka, 1973; Benveniste, 1987) are the most popular and widely used methods. The notion of an effective field in which each particle is located

is a basic concept of such powerful micromechanical methods as the methods of self-consistent fields and effective fields (see for references Kanaun and Levin, 1994; Buryachenko, 2001). The "quasi-crystalline" approximation by Lax (1952) is often used for truncation of the hierarchy of system of integral equations involved leading to neglect of direct multiparticle interactions of inclusions. This noninteraction deficiency was overcome recently by the multiparticle effective field method (MEFM) which includes as particular cases the well-known methods of mechanics of strongly heterogeneous media (such as the effective medium and the mean field methods) (see for references Buryachenko, 2001). The MEFM is based on the theory of functions of random variables and Green's functions. Within this method a hierarchy of statistical moment equations for conditional averages of the stresses in the inclusions is derived. The hierarchy is established by introducing the notion of an effective field. In this way the interaction of different inclusions is taken directly into account.

It is known that using a one point probability density (volume fraction) can provide only a rough estimation of the bounds of the effective properties and statistical averages of stresses in the constitutive equations of composite materials. More informative characteristics of the point set are obtained using statistical second-order quantities (such as two-point probability density, second-order intensity function, and nearest neighbor distribution) which examine the association of a point relative to other points. These statistical distributions have been used for generating concrete realizations of the location of a final number of interacting inclusions and analyzed using elastic analysis (see e.g. Ghosh et al., 1997; Pyrz and Bochenek, 1998). More rigorous estimations of the statistical average of stress fields in the constituents and therefore of effective elastic moduli are based on the statistical averaging of random integral equations for an infinite number of inclusions where the configuration is described by statistical second-order functions (see for references Buryachenko, 2001; Torquato, 2002a,b). In particular, in the current paper we demonstrated the strong dependence of effective moduli on the concrete form of the radial distribution function and demonstrated strong differences in effective moduli for apparently similar distributions.

It is noted that the estimation of the effective elastic moduli is a linear problem, with respect to the stress field analyzed which is less sensitive to the local stress distribution than nonlinear micromechanical problems of elastoplastic deformation, fracture, and fatigue of composite materials depending, at least, on mean-square stress fluctuations in the constituents (see e.g. Ponte Castañeda and Suquet, 1998; Buryachenko, 2001; Lipton, 2003). Buryachenko (2001) estimated the second moment of stresses averaged over the volume of the constituents by the use of the radial distribution function (RDF) with application for the analysis of a wide class of nonlinear problems. The estimations of second moment of stresses are defined by both the random stress fluctuations in the components and the inhomogeneity of the stress fields in the constituents which cannot be separated in the framework of the method proposed. However, the method also allows one to estimate the second moment of stresses for interface stresses at each point on the interface between the matrix and fibers. The dispersion of these interface stresses, defined only by stress fluctuations, will be used in this paper for the prediction of the failure initiation. The failure initiation is dependent on the size and the volume fraction of fibers, their surface treatment, matrix and fiber properties. A change of the adhesion properties of the interface, defined by the surface treatment, has a smaller effect on modulus than on strength. Indeed, even poor adhesion between the constituents does not appear to be an important factor as long as the frictional forces between the phases are not exceeded by the interface stress. Because of this, the estimation of the failure initiation envelope of the interface is of practical interest.

The outline of the paper is as follows. In Section 2, the quantitative descriptors of the dispersion of fibers in unidirectional composites will be analyzed in order to describe the pattern of fiber location as observed in test specimens rather than as described by some assumed model. Since generated random packing structures are strongly dependent on the procedure of their generation, we will consider a few popular algorithms and their combinations, adapted for obtaining the most homogeneous configurations and will compare the statistical parameters of configurations generated by the different methods. In Section 3 the

dependence of effective elastic properties of fiber composites on the radial distribution functions estimated from experimental data as well as from the ensembles generated by each proposed method is discussed. In Section 4 the statistical moments of stresses for the ensemble of inclusions as well as the second moment of interface stresses are derived. Section 5 determines the local and effective failure envelopes for matrix microcracking and interface failure, and in Section 6 numerical examples are presented.

2. Preliminaries

Let stresses and strains be related to each other via the constitutive equation

$$\boldsymbol{\sigma}(\mathbf{x}) = \mathbf{L}(\mathbf{x})\boldsymbol{\varepsilon}(\mathbf{x}), \tag{2.1}$$

where $\mathbf{L}$ is the fourth-order anisotropic elasticity tensor, which for isotropic materials is given by

$$\mathbf{L} = (dK_{[d]}, 2G_{[d]}) \equiv dK_{[d]}\mathbf{N}_1 + 2G_{[d]}\mathbf{N}_2, \quad \mathbf{N}_1 = \boldsymbol{\delta} \otimes \boldsymbol{\delta}/d, \quad \mathbf{N}_2 = \mathbf{I} - \mathbf{N}_1 \tag{2.2}$$

$K_{[d]}$ and $G_{[d]}$ are the bulk and shear moduli, respectively; $\boldsymbol{\delta}$ and $\mathbf{I}$ are the unit second-order and fourth-order tensors. The interrelations among the planar and three-dimensional moduli can be found, e.g. in Torquato (2002a). For example, for plane strain $G_{[2]} = G_{[3]}$, $K_{[2]} = K_{[3]} + G_{[3]}/3$, $E_{[2]} = E_{[3]}/(1 + \nu_{[3]})(1 - \nu_{[3]})$, $\nu_{[2]} = \nu_{[3]}/(1 - \nu_{[3]})$ and for plane stress $G_{[2]} = G_{[3]}$, $K_{[2]} = 9K_{[3]}G_{[3]}/(3K_{[3]} + 4G_{[3]})$, $E_{[2]} = E_{[3]}$, $\nu_{[2]} = \nu_{[3]}$ where E and ν are the Young modulus and Poisson's ratio. The local strain and stress tensors satisfy the linearized strain-displacement relations and the equilibrium equation, respectively. We consider a mesodomain w, subjected to the uniform traction boundary conditions.

In the mesodomain w containing a set $X = (V_i, \mathbf{x}_i, \omega_i)$ $(i = 1, 2, \ldots)$ of ellipsoids v_i with characteristic functions V_i, centers x_i, semi-axes a_i^j $(j = 1, 2, 3)$ and an aggregate of Euler angles ω_i, a characteristic function W is defined. It is assumed that all inclusions have identical mechanical and geometrical properties and are grouped into the component $v^{(1)}$. In the matrix $v^{(0)} = w \setminus v^{(1)}$ and in the inclusions $v^{(1)}$ the tensor $\mathbf{f}(\mathbf{x})(\mathbf{f} = \mathbf{L}, \mathbf{M}, \mathbf{M} \equiv \mathbf{L}^{-1})$ is assumed to be constant: $\mathbf{f}(\mathbf{x}) = \mathbf{f}^{(0)}$ for $\mathbf{x} \in v^{(0)}$ and $\mathbf{f}(\mathbf{x}) = \mathbf{f}^{(0)} + \mathbf{f}_1(\mathbf{x}) = \mathbf{f}^{(0)} + \mathbf{f}_1^{(1)}$ for $\mathbf{x} \in v^{(1)}$. The upper index of the material properties tensor put in parentheses shows the number of the respective component. The subscript 1 denotes a jump of the corresponding quantity (e.g. of the material tensor). The phases are perfectly bonded.

For random structure composites, we introduce a conditional probability density $\varphi(v_m, \mathbf{x}_m | v_i, \mathbf{x}_i)$, which describes the probability density of finding the mth inclusion in the domain v_m with the center $\mathbf{x}_m$, the inclusions in the domains v_i with the centers $\mathbf{x}_i \neq \mathbf{x}_m$ being treated as fixed. We will consider statistically homogeneous media, when all the random quantities under discussion are statistically homogeneous and, hence, the ensemble averaging could be replaced by volume averaging

$$\langle(\cdot)\rangle = \bar{w}^{-1} \int (\cdot) W(\mathbf{x})\, \mathrm{d}\mathbf{x}, \quad \langle(\cdot)\rangle^{(k)} = [\bar{v}^{(k)}]^{-1} \int (\cdot) V^{(k)}(\mathbf{x})\, \mathrm{d}\mathbf{x}, \tag{2.3}$$

where $\sum V^{(1)} = \sum V_i$, $i = 1, 2, \ldots$, and the bar appearing above the region represents its measure, e.g. $\bar{v} \equiv \mathrm{mes}\, v$. Of course, $\varphi(v_m, \mathbf{x}_m |; v_i, \mathbf{x}_i) = 0$ for values of $\mathbf{x}_m$ lying inside the "included volumes" $\cup v_{im}^0 (m = 1, \ldots, n)$, where $v_{im}^0 \supset v_m$ with characteristic functions V_{im}^0 (since inclusions cannot overlap). $\varphi(v_i, \mathbf{x})$ is a number density $n(\mathbf{x})$ of inclusions in the point $\mathbf{x}$ and $c^{(1)} = c^{(1)}(\mathbf{x})$ is the concentration, i.e. volume fraction, of the component $v^{(1)}$ in the point $\mathbf{x}$: $c^{(1)}(\mathbf{x}) = \langle V^{(1)}\rangle(\mathbf{x}) = \bar{v}_i n(\mathbf{x})$, $c^{(0)}(\mathbf{x}) = 1 - \langle V^{(1)}\rangle(\mathbf{x})$. Here the notation $\langle(\cdot)\rangle(\mathbf{x})$ will be used for the average taken for the ensemble of a statistically inhomogeneous field $X = (v_i)$ in the point $\mathbf{x}$. The notation $\langle(\cdot)\rangle_k$ denotes the average over the component $v^{(k)} (k = 0, 1)$. $\varphi(v_i)$ is a number density n of component $v^{(1)} \ni v_i$ and $c^{(k)} (k = 0, 1)$ is the concentration, i.e. volume fraction, of the component $v^{(k)}$: $c^{(1)} = \langle V^{(1)}(\mathbf{x})\rangle = \bar{v}_i n^{(1)} (k = 1;\ i = 1, 2, \ldots)$, $c^{(0)} = 1 - \langle V\rangle$.

Only if the pair distribution function $g(\mathbf{x}_i - \mathbf{x}_m) \equiv \varphi(v_i, \mathbf{x}_i|; v_m, \mathbf{x}_m)/n^{(k)}$ depends on $|\mathbf{x}_m - \mathbf{x}_i|$ it is called the radial distribution function (RDF). The RDFs estimated from experimental data utilized a digital image processing technique to identify fiber centroids and describe the stochastic structure of the material through estimation of the statistical parameters and functions that describe the radial fiber distribution (see Buryachenko et al., 2003). An example of one of the micrographs for a carbon fiber-reinforced epoxy composite ($c^{(1)} = 0.65$) used to determine the experimental RDF is shown in the Fig. 1. The numerical simulation was carried out by the modified collective rearrangement model (CRM) accompanied by the random shaking procedure, creating the most homogeneous and mixed structures that do not depend on the initial protocol of particle generations (see for detail Buryachenko et al., 2003).

In Fig. 2 we compare the RDF estimated from the experimental fiber centroid data with that from numerical simulation by the CRM, as well as the RDF represented analytically by

$$g(\mathbf{x}_i - \mathbf{x}_q) \equiv H(r - 2a), \tag{2.4}$$

$$g(\mathbf{x}_i - \mathbf{x}_q) = H(r - 2a)\left\{1 + \frac{4c}{\pi}\left[\pi - 2\sin^{-1}\left(\frac{r}{4a}\right) - \frac{r}{2a}\sqrt{1 - \frac{r^2}{16a^2}}\right]H(4a - r)\right\}, \tag{2.5}$$

where H denotes the Heaviside step function, $r \equiv |\mathbf{x}_i - \mathbf{x}_q|$ is the distance between the nonintersecting inclusions v_i and v_q, and c is the area fraction of circle inclusions with the radius a. The so-called well-stirred approximation for the RDF differs from the RDF for a Poisson distribution by the availability of "included volume" with the center $\mathbf{x}_i$ where $g(\mathbf{x}_i - \mathbf{x}_q) \equiv 0$. Eq. (2.5) (see Torquato and Lado, 1992; Hansen and McDonald, 1986) takes into account a neighboring order in the distribution of the inclusions. Fig. 2 shows a good fit between RDFs estimated from experimental data and from numerical simulation and are substantially dissimilar from the curves (2.4) and (2.5). The experimental data for a carbon fiber-reinforced epoxy composite were obtained by averaging over ten materials specimens each of the 10 samples containing around 2000 fibers (see for details Buryachenko et al., 2003). In Fig. 3 the functional dependences of the RDF on the relative radius for four different volume concentrations are presented. As can be seen, the experimental data is close to the numerical simulation but not close to the predictions from using Eq. (2.4) or (2.5) as compared to the measured RDF.

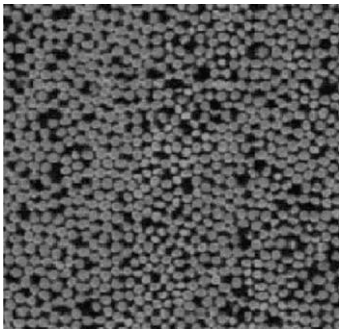

Fig. 1. Typical micrograph of fiber reinforced composite specimen used in determining experimental radial distribution function $c^{(1)} = 0.65$.

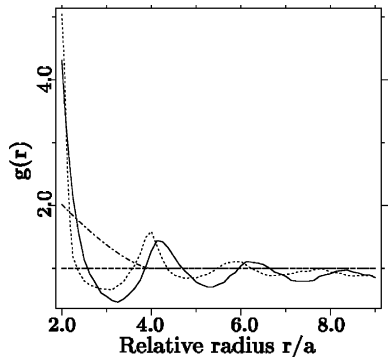

Fig. 2. The radial distribution functions $g(r)$ vs relative radius r/a estimated by the numerical simulation (solid curve), from experimental data (dotted curve), by the analytical approximation (2.5) (dot-dashed curve), by the well-stirred approximation (2.4) (dashed curve).

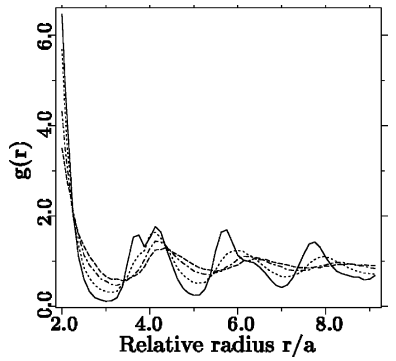

Fig. 3. The radial distribution functions $g(r)$ vs relative radius r/a estimated by the modified CRM at $c = 0.60$ (dashed curve), $c = 0.65$ (dot-dashed curve), $c = 0.70$ (dotted curve), $c = 0.75$ (solid curve).

3. Effective elastic properties

First, we will summarize the basic assumptions and the final formulae of the multiparticle effective field method (MEFM) for estimation of effective elastic moduli. For a detailed discussion and numerous references for this and related methods, the reader is referred to Buryachenko (2001).

The general integral equation is known (see for references Buryachenko, 2001)

$$\boldsymbol{\sigma}(\mathbf{x}) = \langle \boldsymbol{\sigma} \rangle + \int \boldsymbol{\Gamma}(\mathbf{x}-\mathbf{y})[\boldsymbol{\eta}(\mathbf{y}) - \langle \boldsymbol{\eta}(\mathbf{y}) \rangle]\, d\mathbf{y}, \tag{3.1}$$

where the tensor $\boldsymbol{\eta}(\mathbf{x}) = \mathbf{M}_1(\mathbf{y})\boldsymbol{\sigma}(\mathbf{y})$ is called the stress polarization tensor, and the notation $\langle(\cdot)\rangle$ will be used for the statistical average. The integral operator kernel $\boldsymbol{\Gamma}(\mathbf{x}-\mathbf{y}) \equiv -\mathbf{L}^{(0)}[\mathbf{I}\boldsymbol{\delta}(\mathbf{x}-\mathbf{y}) + \nabla\nabla\mathbf{G}(\mathbf{x}-\mathbf{y})\mathbf{L}^{(0)}]$ is defined by the Green tensor $\mathbf{G}$ of the Lame' equation of a homogeneous medium with an elasticity tensor $\mathbf{L}^{(0)} : \nabla\{\mathbf{L}^{(0)}[\nabla \otimes \mathbf{G}(\mathbf{x}) + (\nabla \otimes \mathbf{G})^{\top}]/2\} = -\boldsymbol{\delta}\delta(\mathbf{x})$; $\delta(\mathbf{x})$ is the Dirac delta function.

After conditional statistical averaging Eq. (3.1), turns into an infinite system of integral equations. In order to close and approximately solve this system we now apply the MEFM hypotheses

(H1) *Each inclusion v_i has an ellipsoidal form and is located in the field*

$$\bar{\boldsymbol{\sigma}}_i(\mathbf{y}) \equiv \bar{\boldsymbol{\sigma}}(\mathbf{x}_i) \quad (\mathbf{y} \in v_i) \tag{3.2}$$

which is homogeneous over the inclusion v_i.

(H2) *Each pair of the inclusions v_i and v_j is located in an effective field $\widehat{\boldsymbol{\sigma}}(\mathbf{x})_{i,j}$ and*

$$\langle \widehat{\boldsymbol{\sigma}}(\mathbf{x})_{i,j} \rangle_k = \langle \bar{\boldsymbol{\sigma}}_k \rangle(\mathbf{x}) = \text{const.} \quad (\mathbf{x} \in v_k, k = i, j). \tag{3.3}$$

According to hypothesis (H1) and to Eshelby's theorem we get ($\mathbf{x} \in v_i$)

$$\boldsymbol{\sigma}(\mathbf{x}) = \mathbf{B}\bar{\boldsymbol{\sigma}}(\mathbf{x}), \quad \bar{v}_i \boldsymbol{\eta}_i(\mathbf{x}) = \mathbf{R}\bar{\boldsymbol{\sigma}}(\mathbf{x}), \tag{3.4}$$

where $\mathbf{R} = \bar{v}_i \mathbf{M}_1^{(1)} \mathbf{B}$, $\mathbf{B} = [\mathbf{I} + \mathbf{Q}\mathbf{M}_1^{(1)}]^{-1}$ and the tensor $\mathbf{Q} \equiv -\langle \boldsymbol{\Gamma} \rangle_{(i)}$ is associated with the well-known Eshelby tensor $\mathbf{S}$ by $\mathbf{S} = \mathbf{I} - \mathbf{M}^{(0)}\mathbf{Q}$. Hereafter $\boldsymbol{\eta}_i \equiv \langle \boldsymbol{\eta}(\mathbf{x}) V_i(\mathbf{x}) \rangle_{(i)}$ is an average over the volume of the inclusion v_i (but not over the ensemble), $\langle (\cdot) \rangle_i \equiv \langle \langle (\cdot) \rangle_{(i)} \rangle$, and the tensors

$$\mathbf{T}_i(\mathbf{y} - \mathbf{x}_i) = \begin{cases} -(\bar{v}_i)^{-1}\mathbf{Q}_i, & \mathbf{y} \in v_i, \\ \langle \boldsymbol{\Gamma}(\mathbf{y} - \mathbf{x}) V_i(\mathbf{x}) \rangle_{(i)}, & \mathbf{y} \notin v_i, \end{cases}, \quad \mathbf{T}_{ij}(\mathbf{x}_i - \mathbf{x}_j) = \langle \mathbf{T}_i(\mathbf{z} - \mathbf{x}_i) \rangle_{(j)} \tag{3.5}$$

($\mathbf{z} \in v_j \neq v_i$) have analytical representations for the spherical inclusions in an isotropic matrix.

The hypotheses (H1), (H2) can be used for an approximate solution of Eq. (3.1) and subsequent estimation of effective elastic moduli in the overall constitutive equation $\langle \boldsymbol{\sigma} \rangle = \mathbf{L}^* \langle \boldsymbol{\sigma} \rangle$:

$$\mathbf{M}^* = \mathbf{M}^{(0)} + \mathbf{Y}\mathbf{R}n, \quad \mathbf{Y}^{-1} = \mathbf{I} - \int \mathscr{T}_{iq}(\mathbf{x}_i - \mathbf{x}_q)\, \mathrm{d}\mathbf{x}_q, \tag{3.6}$$

$$\mathscr{T}_{iq}(\mathbf{x}_i - \mathbf{x}_q) \equiv \mathbf{R}_i n \{ \mathbf{T}_{iq}(\mathbf{x}_i - \mathbf{x}_q)[\mathbf{Z}_{qi} + \mathbf{Z}_{qq}] g(r) - \mathbf{T}_i(\mathbf{x}_i - \mathbf{x}_q) \}, \tag{3.7}$$

where $r = |\mathbf{x}_q - \mathbf{x}_i|$, and the matrix elements $\mathbf{Z}_{qi}$, $\mathbf{Z}_{qq}$ are nondiagonal and diagonal elements, respectively, of the binary interaction matrix $\mathbf{Z}$ for the two inclusions v_q and v_i with the elements of the inverse matrix

$$(\mathbf{Z}^{-1})_{iq} = \mathbf{I}\delta_{iq} - (1 - \delta_{iq})\mathbf{R}_q \mathbf{T}_{iq}(\mathbf{x}_i - \mathbf{x}_q). \tag{3.8}$$

Thus, the effective elastic moduli $\mathbf{L}^*$ explicitly depend on the RDF $g(r)$ and the volume concentration $c = n\bar{v}_i$ of inclusions. Neglecting the binary interaction of inclusions yields

$$\mathbf{Z}_{iq} = \mathbf{I}\delta_{iq} \tag{3.9}$$

reduces the formula (3.7) for the effective elastic moduli to the analogous relation obtained by Mori–Tanaka method which is invariant to the RDF $g(r)$.

4. Statistical moments of stresses in the components

The mean field of elastic stresses inside the inclusions $\langle \boldsymbol{\sigma} \rangle_i$ is obtained from (3.4) and (3.6)

$$\langle \boldsymbol{\sigma} \rangle_i = (\mathbf{M}_1^{(1)})^{-1} \mathbf{D} \boldsymbol{\sigma}^0, \quad \mathbf{D} = \mathbf{R}^{-1}\mathbf{Y}\mathbf{R}, \tag{4.1}$$

where the tensor $\mathbf{D}$ has a simple physical meaning of describing the interaction of neighboring inclusions on the inclusion i : $\langle \bar{\boldsymbol{\sigma}} \rangle_i = \mathbf{D}\boldsymbol{\sigma}^0$. The mean matrix stress follows from the relation:

$$\langle \boldsymbol{\sigma} \rangle_0 = \frac{1}{c^{(0)}} (\boldsymbol{\sigma}^0 - \langle \boldsymbol{\sigma} V \rangle). \tag{4.2}$$

The fourth-rank tensor of the second moment of stresses $\langle \boldsymbol{\sigma} \otimes \boldsymbol{\sigma} \rangle_i$ averaged over the volume of the component $v^{(k)}$, $(k = 0, \ldots, N)$ can be exactly determined by the perturbation method from the functional

dependence of the effective compliance $\mathbf{M}^*$, stored energy U^* and effective eigenstrains β^* on the compliance of the component $v^{(k)}$ (see for references Buryachenko, 2001)

$$\langle \boldsymbol{\sigma} \otimes \boldsymbol{\sigma} \rangle^{(k)} = \frac{1}{c^{(k)}} \frac{\partial \mathbf{M}^*}{\partial \mathbf{M}^{(k)}} \boldsymbol{\sigma}^0 \otimes \boldsymbol{\sigma}^0, \tag{4.3}$$

or in index form:

$$\langle \sigma_{ij} \sigma_{mn} \rangle^{(k)} = \frac{1}{c^{(k)}} \frac{\partial M^*_{pqrs}}{\partial M^{(k)}_{ijmn}} \sigma^0_{pq} \sigma^0_{rs}. \tag{4.4}$$

Relations (4.3), (4.4) have been obtained for any degree of anisotropy of $\mathbf{M}^*$, $\mathbf{M}^{(i)} (i = 0, 1, \ldots, N)$. For isotropic tensors $\mathbf{M}^{(i)} = (3p^{(i)}, 2q^{(i)}) \equiv 3p^{(i)}\mathbf{N}_1 + 2q^{(i)}\mathbf{N}_2$, $(\mathbf{N}_1 = \boldsymbol{\delta} \otimes \boldsymbol{\delta}/3, \mathbf{N}_2 = \mathbf{I} - \mathbf{N}_1)$, we have

$$\langle \sigma_0^2 \rangle^{(k)} = \frac{1}{9c^{(k)}} \frac{\partial M^*_{pqrs}}{\partial p^{(k)}} \sigma^0_{pq} \sigma^0_{rs}, \quad \langle \mathbf{ss} \rangle^{(k)} = \frac{1}{2c^{(k)}} \frac{\partial M^*_{pqrs}}{\partial q^{(k)}} \sigma^0_{pq} \sigma^0_{rs}, \tag{4.5}$$

where $\sigma_0 \equiv \boldsymbol{\delta}\boldsymbol{\sigma}/3$, $\mathbf{s} = \mathbf{N}_2\boldsymbol{\sigma}$. Eq. (4.5) are reduced to the results found by Bobeth and Diener (1986) for macroisotropic composites.

The stress in the vicinity of the inhomogeneities v_i in the matrix $\boldsymbol{\sigma}_i^-(\mathbf{n})$ is given by the formula

$$\boldsymbol{\sigma}_i^-(\mathbf{n}) = \mathbf{B}(\mathbf{n})\boldsymbol{\sigma}_i^+(\mathbf{x}), \tag{4.6}$$

where $\boldsymbol{\sigma}_i^-(\mathbf{n})$ and $\boldsymbol{\sigma}_i^+(\mathbf{x})$ are the limiting stress outside and inside, respectively near the inclusion boundary $\partial v_i : \boldsymbol{\sigma}_i^-(\mathbf{n}) = \lim \boldsymbol{\sigma}(\mathbf{y})$, $\boldsymbol{\sigma}_i^+ = \lim \boldsymbol{\sigma}(\mathbf{z})$, $\mathbf{y} \to \mathbf{x}$, $\mathbf{z} \to \mathbf{x}$, $\mathbf{y} \in v_0$, $\mathbf{z} \in v_i$, $\mathbf{x} \in \partial v_i$, $\mathbf{n} \perp \partial v_i$; $\mathbf{n}$ is the unit outward normal vector on ∂v_i. The relation (4.6) is valid for any geometric form of the inclusion v_i. The tensor $\mathbf{B}(\mathbf{n})$ only depends on elastic properties of contacted materials and on the direction of the normal $\mathbf{n}$:

$$\mathbf{B}(\mathbf{n}) = \mathbf{L}^-[\mathbf{I} + \mathbf{U}(\mathbf{n})^-(\mathbf{L}^+ - \mathbf{L}^-)]\mathbf{M}^+, \tag{4.7}$$

where $U(\mathbf{n})^{\pm}_{klmn} = [n_k G(\mathbf{n})^{\pm}_{lm} n_n]_{(kl)(mn)}$, and the matrix $\mathbf{G}(\mathbf{n})^- = [\mathbf{L}(\mathbf{n})^-]^{-1}$ is the inverse of the matrix $\mathbf{L}(\mathbf{n})^- = \mathbf{L}^-\mathbf{n} \otimes \mathbf{n}$. Here the symbol + and − relate to the different boundary sides. In particular for an isotropic medium with the elastic modulus (2.2) an inversion of the matrix $\mathbf{L}(\mathbf{n})$ may be simplified and we obtain

$$L(n)_{kl} = \mu\delta_{kl} + \left(k + \frac{\mu}{3}\right) n_k n_l, \quad G(n)_{kl} = \mu^{-1}\left(\delta_{kl} - \frac{2k + \mu}{3k + 4\mu} n_k n_l\right), \tag{4.8}$$

$$U(n)_{klmn} = \frac{1}{2\mu}\left(E_{klmn} - \frac{3k - 2\mu}{3k + 4\mu} n_k n_l n_m n_n\right). \tag{4.9}$$

Substitution of Eq. (4.1) into Eq. (4.6) leads to the estimation of statistical averages of stresses in the matrix in the vicinity of inclusions at a point $\mathbf{x} \in \partial v_i$

$$\langle \boldsymbol{\sigma}_i^-(\mathbf{n}) \rangle_{\mathbf{x}} = \mathbf{B}(\mathbf{n})\mathbf{B}\mathbf{D}\langle \boldsymbol{\sigma} \rangle. \tag{4.10}$$

Moreover, Buryachenko (2001) has obtained the estimation of the second moment of these stresses

$$\langle \boldsymbol{\sigma}_i^-(\mathbf{n}) \otimes \boldsymbol{\sigma}_i^-(\mathbf{n}) \rangle_{\mathbf{x}} = [\boldsymbol{\mathscr{B}}^{*\mathrm{per}}(\mathbf{n}) \otimes \boldsymbol{\mathscr{B}}^{*\mathrm{per}}(\mathbf{n})]\langle \boldsymbol{\sigma} \rangle \otimes \langle \boldsymbol{\sigma} \rangle, \tag{4.11}$$

where one introduced the interface stress concentrator factor

$$[\boldsymbol{\mathscr{B}}^{*\mathrm{per}}(\mathbf{n}) \otimes \boldsymbol{\mathscr{B}}^{*\mathrm{per}}(\mathbf{n})] = \frac{1}{c^{(k)}} [\mathbf{B}(\mathbf{n}) \otimes \mathbf{B}(\mathbf{n})] \frac{\partial \mathbf{M}^*}{\partial \mathbf{M}^{(k)}}. \tag{4.12}$$

Neglecting of stress fluctuations in the fibers $\langle \boldsymbol{\sigma} \otimes \boldsymbol{\sigma} \rangle_{(1)} \equiv \langle \boldsymbol{\sigma} \rangle_{(1)} \otimes \langle \boldsymbol{\sigma} \rangle_{(1)}$ leads to the simplification of Eq. (4.11)

$$[\mathscr{B}^{*\mathrm{per}}(\mathbf{n}) \otimes \mathscr{B}^{*\mathrm{per}}(\mathbf{n})] = \mathbf{B}(\mathbf{n})\mathbf{B}\mathbf{D} \otimes \mathbf{B}(\mathbf{n})\mathbf{B}\mathbf{D}. \tag{4.13}$$

The second moment of stresses can be estimated not just by the perturbation method (4.3), but also by the method of integral equations

$$\langle \boldsymbol{\sigma} \otimes \boldsymbol{\sigma} \rangle_i = \langle \boldsymbol{\sigma} \rangle_i \otimes \langle \boldsymbol{\sigma} \rangle_i + \int [\mathbf{B}\mathbf{T}_{ip}(\mathbf{x}_i - \mathbf{x}_p)\langle \boldsymbol{\eta} \rangle_p \bar{v}_p] \otimes [\mathbf{B}\mathbf{T}_{ip}(\mathbf{x}_i - \mathbf{x}_p)\langle \boldsymbol{\eta} \rangle_p \bar{v}_q] \cdot \varphi(v_p, \mathbf{x}_p|; v_i, \mathbf{x}_i)\, \mathrm{d}\mathbf{x}_p. \tag{4.14}$$

It was demonstrated (see for references Buryachenko, 2001) that both Eqs. (4.3) and (4.14) lead to similar results. Then the second moment of interface stresses can be presented in the form (4.11)

$$\langle \boldsymbol{\sigma}_i^-(\mathbf{n}) \otimes \boldsymbol{\sigma}_i^-(\mathbf{n}) \rangle_{\mathbf{x}} = [\mathscr{B}^{*\mathrm{int}}(\mathbf{n}) \otimes \mathscr{B}^{*\mathrm{int}}(\mathbf{n})] \langle \boldsymbol{\sigma} \rangle \otimes \langle \boldsymbol{\sigma} \rangle, \tag{4.15}$$

where

$$\begin{aligned}[\mathscr{B}^{*\mathrm{int}}(\mathbf{n}) \otimes \mathscr{B}^{*\mathrm{int}}(\mathbf{n})] \\ = \mathbf{B}(\mathbf{n})\mathbf{B}\mathbf{D} \otimes \mathbf{B}(\mathbf{n})\mathbf{B}\mathbf{D} + \int \mathbf{B}(\mathbf{n})\mathbf{B}\mathbf{T}_{ip}(\mathbf{x}_i - \mathbf{x}_p)\mathbf{R} \otimes \mathbf{B}(\mathbf{n})\mathbf{B}\mathbf{T}_{ip}(\mathbf{x}_i - \mathbf{x}_p)\mathbf{R}\varphi(v_p, \mathbf{x}_p|; v_i, \mathbf{x}_i)\, \mathrm{d}\mathbf{x}_p.\end{aligned} \tag{4.16}$$

The representations (4.15) and (4.16) were obtained with additional simplifying assumptions for the hypothesis (H1) and (H2) which are used for the concrete estimation of the second moment of stresses by the perturbation method (4.11) and (4.12). More accurate cumbersome integral representations generalizing Eq. (4.16) were obtained by Buryachenko and Rammerstorfer (1998).

5. Effective failure envelope

5.1. Local failure envelope

The failure analysis of composite materials considers the initiation and accumulation of damage occuring in each phase of the material and involves several types of local degradation processes including matrix microcracking (type I), interfacial debonding (type II), and fiber breakages (type III), etc. Generally, these failure mechanisms may initiate concurrently in an early loading stage and progressively accumulate inside the materials (see for references and detail Kutlu and Chang, 1995; Meraghni et al., 1996; Reddy, 1994; Desrumaux et al., 2001).

The first type of damage processes are those that relate to matrix degradation. They include matrix microcracking and pseudo-delamination. The second type of degradation models describe interfacial decohesion and related mechanisms, such as fiber matrix friction and fiber pull-out processes. Let us assume that the well-known tensor-polynomial strength criterion by Tsai and Wu (1971) describes the initiation of failure mechanisms of the types I and III for each component, i.e. the equivalent stress is given by

$$\boldsymbol{\Pi}^{(i)}(\boldsymbol{\sigma}) = \boldsymbol{\Pi}^{1(i)}\boldsymbol{\sigma} + \boldsymbol{\Pi}^{2(i)}(\boldsymbol{\sigma} \otimes \boldsymbol{\sigma}) + \boldsymbol{\Pi}^{3(i)}(\boldsymbol{\sigma} \otimes \boldsymbol{\sigma} \otimes \boldsymbol{\sigma}) + \cdots = 1, \tag{5.1}$$

where $i = 0, 1, \ldots$, and the second-, fourth- and sixth-rank tensors of strength $\boldsymbol{\Pi}^1$, $\boldsymbol{\Pi}^2$, $\boldsymbol{\Pi}^3$ are expressed through technical strength parameters for different classes of material symmetry (Theocaris, 1991; Zhiging and Tennysin, 1989). It should be mentioned that in the Section 5.1, the tensor $\boldsymbol{\sigma} = \boldsymbol{\sigma}(\mathbf{x})$ stands the local stresses in the composite material. The criterion (5.1) includes the Von Mises equivalent stress criterion ($\sigma_y^2 = \mathrm{const.}$)

$$\boldsymbol{\Pi}(\boldsymbol{\sigma}) = \frac{1}{2\sigma_y^2}[(\sigma_{11} - \sigma_{22})^2 + (\sigma_{22} - \sigma_{33})^2 + (\sigma_{11} - \sigma_{33})^2] + 3[(\sigma_{12})^2 + (\sigma_{13})^2 + (\sigma_{23})^2] = 1. \tag{5.2}$$

The modeling of global composite behavior necessarily requires the consideration of interface degradation in addition to the matrix and fiber phase degradation (5.1). This requires not only the calculation of the stress at the interface, but equally the identification and the application of a local failure criterion. In a similar manner with Eq. (5.1) we can present a tensor-polynomial failure criterion for the interface failure initiation

$$\mathbf{\Pi}_a^{(i)}(\mathbf{n},\boldsymbol{\sigma}) = \mathbf{\Pi}_a^{1(i)}(\mathbf{n})\boldsymbol{\sigma}^-(\mathbf{n}) + \mathbf{\Pi}_a^{2(i)}(\mathbf{n})[\boldsymbol{\sigma}^-(\mathbf{n}) \otimes \boldsymbol{\sigma}^-(\mathbf{n})] + \cdots = 1, \tag{5.3}$$

where $\boldsymbol{\sigma}^-(\mathbf{n})$ is the limiting stresses within the matrix near the inclusion boundary $\mathbf{x} \in \partial v_i$ with the unit outward normal vector $\mathbf{n}$. Generally speaking adhesion strength parameters $\mathbf{\Pi}_a^{1(i)}(\mathbf{n})$, $\mathbf{\Pi}_a^{2(i)}(\mathbf{n})$, $\mathbf{\Pi}_a^{3(i)}(\mathbf{n})$, which convey the normal and the shear debonding at the interface between the matrix and the fibers, differ from $\mathbf{\Pi}^{1(i)}$, $\mathbf{\Pi}^{2(i)}$, $\mathbf{\Pi}^{3(i)}$.

We will present now popular local criteria that convey the normal and the shear debonding at the interface between the matrix and the fibers. Determination of the failure characteristics of the interface is carried out through a mechanical characterization of the interfacial resistance by means of specific tests such as fiber pull-out, fiber push-out, etc. The interface stresses $\boldsymbol{\sigma}_{\mathbf{n}}^- \equiv \boldsymbol{\sigma}^-(\mathbf{n})\mathbf{n}$ can be partitioned as $\boldsymbol{\sigma}_{\mathbf{n}}^- = \mathbf{N}^{\mathbf{n}}\boldsymbol{\sigma}^-(\mathbf{n}) + \mathbf{T}^{\mathbf{n}}\boldsymbol{\sigma}^-(\mathbf{n})$, where $\mathbf{N}^{\mathbf{n}}$ and $\mathbf{T}^{\mathbf{n}}$ are the three-rank functions of the normal $\mathbf{n}$ such that

$$N_{ikl}^{\mathbf{n}} = n_i n_k n_l, \quad T_{ikl}^{\mathbf{n}} = \frac{1}{2}(\delta_{ik}n_l + \delta_{il}n_k) - n_i n_k n_l, \tag{5.4}$$

where the tensors $N_{ikl}^{\mathbf{n}}$ and $T_{ikl}^{\mathbf{n}}$ symmetrical under the interchanges $k \leftrightarrow l$ generate the normal $\boldsymbol{\sigma}_n^- = \mathbf{N}^{\mathbf{n}}\boldsymbol{\sigma}^-(\mathbf{n})$ and tangential components $\boldsymbol{\sigma}_\tau^- = \mathbf{T}^{\mathbf{n}}\boldsymbol{\sigma}^-(\mathbf{n})$ of the traction $\boldsymbol{\sigma}^-\mathbf{n}$ with the magnitudes $\sigma_n \equiv \|\boldsymbol{\sigma}_n^-\| = \sigma_{kl}^- n_k n_l$ and $\sigma_\tau \equiv \|\boldsymbol{\sigma}_\tau^-\| = \sqrt{\sigma_{kl}^-\sigma_{kl}^- - (\sigma_n)^2}$, respectively.

In a simple maximum stress criterion, the normal σ_n and tangential σ_τ components are compared to maximum values $\sigma_n^{\max}$ and $\sigma_\tau^{\max}$ characterizing the interface, and the failure tensors $\mathbf{\Pi}_a^{2(i)}(\mathbf{n})$ have a form

$$\bar{\mathbf{\Pi}}_a^{2(i)}(\mathbf{n}) = \max\left[\frac{\|\mathbf{N}^{\mathbf{n}}\boldsymbol{\sigma}^-(\mathbf{n})\|}{\sigma_n^{\max}}, \frac{\|\mathbf{T}^{\mathbf{n}}\boldsymbol{\sigma}^-(\mathbf{n})\|}{\sigma_\tau^{\max}}\right] = \max\left[\frac{\sigma_n}{\sigma_n^{\max}}, \frac{\sigma_\tau}{\sigma_\tau^{\max}}\right] = 1. \tag{5.5}$$

Other type of criteria taking into account the friction problem were considered by a number of authors (see for references Mura et al., 1996). The Coulomb form of the criterion (see Arnould, 1982) permits the introduction of the friction coefficient at the interface by the use of a linear combination between the normal and the shear interface stresses

$$\check{\mathbf{\Pi}}_a^{2(i)}(\mathbf{n}) = \frac{\|\mathbf{N}^{\mathbf{n}}\boldsymbol{\sigma}^-(\mathbf{n})\|}{\sigma_n^{\max}} + \frac{\|\mathbf{T}^{\mathbf{n}}\boldsymbol{\sigma}^-(\mathbf{n})\|}{\sigma_\tau^{\max}} = 1. \tag{5.6}$$

Logical generalization of tensor-polynomial criteria (5.1) to the interface failure initiation was proposed by Sun and Zhou (1988) (see also Kwon and Eren, 2000) for the cylindrical fibers, which in our more general notations has a form

$$\hat{\mathbf{\Pi}}_a^{2(i)}(\mathbf{n}) = \frac{(\mathbf{N}^{\mathbf{n}}\boldsymbol{\sigma}^-(\mathbf{n}))(\mathbf{N}^{\mathbf{n}}\boldsymbol{\sigma}^-(\mathbf{n}))}{(\sigma_n^{\max})^2} + \frac{(\mathbf{T}^{\mathbf{n}}\boldsymbol{\sigma}^-(\mathbf{n}))(\mathbf{T}^{\mathbf{n}}\boldsymbol{\sigma}^-(\mathbf{n}))}{(\sigma_\tau^{\max})^2} = 1. \tag{5.7}$$

The criterion (5.7) can be recast in the tensor-polynomial form (5.3) with the tensors $\mathbf{\Pi}_a^{2(i)}(\mathbf{n}) \equiv \mathbf{0}$ and

$$\mathbf{\Pi}_{a|ijkl}^{2(i)}(\mathbf{n}) = \left[\frac{1}{(\sigma_n^{\max})^2} - \frac{1}{(\sigma_\tau^{\max})^2}\right] n_i n_j n_k n_l + \frac{1}{4(\sigma_\tau^{\max})^2}(\delta_{ik}n_{jl} + \delta_{il}n_{jk} + \delta_{jl}n_{ik} + \delta_{jk}n_{il}). \tag{5.8}$$

Because the criteria (5.5)–(5.7) should predict the identical stresses of the failure initiation at the pure local normal and shear stresses then the empirical interfacial strengths corresponding to tension and shear should

be the same in the criteria (5.5)–(5.7), and, therefore, the failure envelope (5.7) is inserted between the failure surfaces (5.5) and (5.6)

$$\check{\mathbf{\Pi}}_a^{2(i)}(\mathbf{n}) < \hat{\mathbf{\Pi}}_a^{2(i)}(\mathbf{n}) < \bar{\mathbf{\Pi}}_a^{2(i)}(\mathbf{n}), \tag{5.9}$$

where the equalities

$$\check{\mathbf{\Pi}}_a^{2(i)}(\mathbf{n}) = \hat{\mathbf{\Pi}}_a^{2(i)}(\mathbf{n}) = \bar{\mathbf{\Pi}}_a^{2(i)}(\mathbf{n}) \tag{5.10}$$

in general hold just for the normal $\mathbf{n}$ with either the pure normal or pure tangential local loading

$$\boldsymbol{\sigma}^-(\mathbf{n}) \equiv \mathbf{N}^{\mathbf{n}}\boldsymbol{\sigma}^-(\mathbf{n}) \quad \text{or} \quad \boldsymbol{\sigma}^-(\mathbf{n}) \equiv \mathbf{T}^{\mathbf{n}}\boldsymbol{\sigma}^-(\mathbf{n}). \tag{5.11}$$

The equalities also hold in some particular cases of correlations between the elastic and strength properties of constitutives. For example, the equalities (5.10) are valid for any $\mathbf{n}$ for the limiting type of soft fibers (hole, $\mathbf{L}^{(1)} \equiv \mathbf{0}$) when $\boldsymbol{\sigma}_{\mathbf{n}}^- \equiv \mathbf{0}$ and the interface failure is degenerated into the failure of the matrix in the vicinity of the interface. In another limiting case of perfect sliding $\sigma_\tau^{\max} = 0$ (see for references Mura et al., 1996) the equality is also valid for any $\mathbf{n}$. Moreover, the last statement also holds if under the failure initiation one understands the normal debonding $(\mathbf{u}^+ - \mathbf{u}^-)\mathbf{n} > 0$.

It should be mentioned that the transverse strength of the reinforced fiber is usually significantly higher than that of the matrix. The popular assumption is that the strengths of the interface and the matrix are equal (i.e. the bonding between fiber and matrix is assumed to be perfect, see e.g. Ghassemieh and Nassehi, 2001). As an approximation, $\sigma_\tau^{\max}$ is also taken to be a half of $\sigma_n^{\max}$ as usually assumed in a homogeneous isotropic material (see e.g. Kwon and Eren, 2000). In light of the heuristic level of justification, the importance of the fundamental experimental work by Tandon et al. (in press) can scarcely be exaggerated. They have used the single-fiber cruciform test to characterize the initiation of fiber-matrix interface failure in a model composite with the interface subjected to a combined state of transverse and shear stress at a location away from a crack tip or free edge. The elimination of the free-edge effect that requires modeling of a stress singularity, was accomplished by utilizing a cruciform specimen geometry with the arms containing the embedded fiber inclined at the different angles with respect to unit axial tension. The ratio of the normal and shear loading at the interface was governed by the amount of off-axis angle the fiber made with the loading direction.

5.2. Effective failure envelope

A common way to produce an effective failure envelope for the composite materials is substitution of the component average stress values into the formula (5.1) (Arsenault and Taya, 1987; Reifsnider and Gao, 1991) $(i = 0, 1, \ldots)$

$$\mathbf{\Pi}^*(\boldsymbol{\sigma}) = \max_i [\mathbf{\Pi}^{1(i)}\langle\boldsymbol{\sigma}\rangle_i + \mathbf{\Pi}^{2(i)}(\langle\boldsymbol{\sigma}\rangle_i \otimes \langle\boldsymbol{\sigma}\rangle_i) + \mathbf{\Pi}^{3(i)}(\langle\boldsymbol{\sigma}\rangle_i \otimes \langle\boldsymbol{\sigma}\rangle_i \otimes \langle\boldsymbol{\sigma}\rangle_i) + \cdots] = 1. \tag{5.12}$$

As this takes place, the strength criteria in the formula (5.12) brings us to physically inconsistent results, which will be shown later.

It is believed that the following definition of effective strength surface based on fewer assumptions is more correct (see e.g. Buryachenko, 2001; Ponte Castañeda and Suquet, 1998)

$$\mathbf{\Pi}^*(\boldsymbol{\sigma}) = \max_i [\mathbf{\Pi}^{2(i)}\langle\boldsymbol{\sigma}\rangle_i + \mathbf{\Pi}^{4(i)}\langle\boldsymbol{\sigma} \otimes \boldsymbol{\sigma}\rangle_i + \mathbf{\Pi}^{6(i)}\langle\boldsymbol{\sigma} \otimes \boldsymbol{\sigma} \otimes \boldsymbol{\sigma}\rangle_i + \cdots] = 1, \tag{5.13}$$

where the estimations of average stress moments of different orders $\langle\boldsymbol{\sigma}\rangle_i$, $\langle\boldsymbol{\sigma} \otimes \boldsymbol{\sigma}\rangle_i$, $\langle\boldsymbol{\sigma} \otimes \boldsymbol{\sigma} \otimes \boldsymbol{\sigma}\rangle_i (i = 0, 1, \ldots)$ can be found by the use of the relevant formulae of Section 4.

Let us show the physical consistency of the effective strength criterion (5.13) (in contrast to (5.12)). In fact, let us consider a two-component isotropic composite with isotropic phases. In this case one may

observe that symmetry requires that average stresses inside both components will be hydrostator, one $\langle\sigma_{kl}\rangle_1 \equiv \langle\sigma_{kl}\rangle_0(1-c)/c \equiv \sigma^0_{11}\delta_{kl}$; in so doing the microstructure of and the method of calculation of average stresses inside the components (for example (4.1) or any other formula) influence the value of scalar σ^0_{11}, but have no effect on the tensor structure of the fields $\langle\boldsymbol{\sigma}\rangle_0$, $\langle\boldsymbol{\sigma}\rangle_1$. Then the composite strength is dictated by the strength of the component which is to be found under conditions of hydrostatic tension and is not determined by the strength of second component. If the strength of the second component falls far short of the strength of the first one, we will obtain an improper prediction of composite strength. In fact, according to (4.5) and (4.16), the average values of second deviator invariant inside each component $\langle\mathbf{ss}\rangle_i \neq 0 (s_{kl} \equiv \sigma_{kl} - \sigma_{nn}\delta_{kl}/3;\ i = 0, 1, \ldots)$. Therefore the composite strength is defined by the strength of second more weak component at the cost of the fluctuations of the stress deviator.

If the possibility of interfacial fracture is taken into account, the macrostrength criterion can be expressed in the following form $(i = 0, 1, \ldots)$

$$\boldsymbol{\Pi}^*_a(\boldsymbol{\sigma}) = \max\left\{\boldsymbol{\Pi}^*(\langle\boldsymbol{\sigma}\rangle), \max_i \max_{\mathbf{n}} \left[\boldsymbol{\Pi}^{1(i)}_a(\mathbf{n})\langle\boldsymbol{\sigma}^-(\mathbf{n})\rangle_x + \boldsymbol{\Pi}^{2(i)}_a(\mathbf{n})\langle\boldsymbol{\sigma}^-(\mathbf{n})\otimes\boldsymbol{\sigma}^-(\mathbf{n})\rangle_x + \cdots\right]\right\} = 1, \tag{5.14}$$

where $\langle\boldsymbol{\sigma}^-(\mathbf{n})\rangle_x$, $\langle\boldsymbol{\sigma}^-(\mathbf{n})\otimes\boldsymbol{\sigma}^-(\mathbf{n})\rangle_x$, and are the statistical moments of limiting stresses within the matrix near the inclusion boundary $\mathbf{x} \in \partial v_i$ with the unit outward normal vector $\mathbf{n}$ (4.10) and (4.11).

In particular, exploring the local failure envelope (5.7) yields the effective failure criterion

$$\boldsymbol{\Pi}^*_a(\boldsymbol{\sigma}) = \max\left\{\boldsymbol{\Pi}^*(\langle\boldsymbol{\sigma}\rangle), \max_{\mathbf{n}}\left[\frac{\mathbf{N}^{\mathbf{n}}\boldsymbol{\mathscr{B}}^{*\mathrm{per}}(\mathbf{n})\otimes\mathbf{N}^{\mathbf{n}}\boldsymbol{\mathscr{B}}^{*\mathrm{per}}(\mathbf{n})}{(\sigma^{\max}_n)^2} + \frac{\mathbf{T}^{\mathbf{n}}\boldsymbol{\mathscr{B}}^{*\mathrm{per}}(\mathbf{n})\otimes\mathbf{T}^{\mathbf{n}}\boldsymbol{\mathscr{B}}^{*\mathrm{per}}(\mathbf{n})}{(\sigma^{\max}_\tau)^2}\right]\langle\boldsymbol{\sigma}\rangle\otimes\langle\boldsymbol{\sigma}\rangle\right\}. \tag{5.15}$$

6. Numerical results

This section attempts to quantitatively investigate the performance of the present approach to the failure analysis of fiber composites. The results are directly compared with solutions extracted from simplified assumptions (such as Mori–Tanaka approach as well as hypothesis of a homogeneity of stresses in the constituents) and they are presented in order to place the advantages and limitations of the refined approach in evidence.

At first, in order to demonstrate the comparison of the available experimental data with the prediction capability of the proposed method, we will consider the estimation of the effective elastic moduli $\mathbf{L}^*$ (3.8). Assume the matrix is epoxy resin ($k^{(0)} = 4.27$ GPa and $\mu^{(0)} = 1.53$ GPa) which contains circular glass fibers that are all identical ($k^{(1)} = 50.89$ GPa and $\mu^{(1)} = 35.04$ GPa). Four different radial distribution functions for the inclusions will be examined (see Torquato and Lado, 1992; Hansen and McDonald, 1986). The effective shear moduli μ^* (GPa) for composite materials with the mentioned elastic properties of constituents and the different RDF are presented in Fig. 4. As can be seen, the use of the approach (3.7) based on the quasi-crystalline approximation (3.9) (also called Mori–Tanaka (MT) approach) leads to an underestimate of the effective shear modulus by 1.85 times for $c = 0.7$ compared with the experimental data. Much better approximations are given by the MEFM (3.6)–(3.8) which shows good agreement with the experimental data provided by Lee and Mykkanen (1987). In the MEFM model, the best fit is obtained using the RDF simulated by the modified CRM.

For failure analysis, let us consider an isotropic composite made from the epoxy matrix and SCS-0 fibers. Both components are described by isotropic elastic properties (2.2) with the mechanical constants as usually found in the literature (see Tandon et al., in press): $k^{(0)} = 3.82$ GPa, $\mu^{(0)} = 1.74$ GPa, $k^{(1)} = 190.47$ GPa, $\mu^{(1)} = 173.914$ GPa, $\sigma^{\max}_n = 34.8$ MPa, $\sigma^{\max}_\tau = 32.5$ MPa. At first we will consider well-stirred

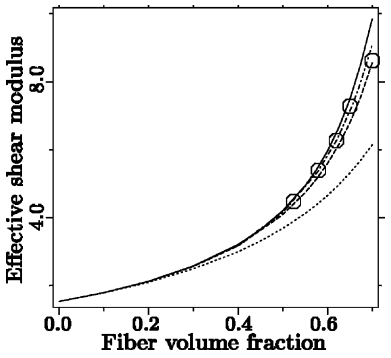

Fig. 4. Variation of the effective shear modulus μ^* (GPa) as a function of a concentration of the inclusions c. Experimental data (○) and curves calculated by Eqs. (3.6)–(3.8) and 2.5 (solid line), by (3.6)–(3.8) with the RDF simulated by the modified CRM (dot-dashed line), by (3.6)–(3.8) and 2.4 (dashed curve), and by the Mori–Tanaka method (dotted line).

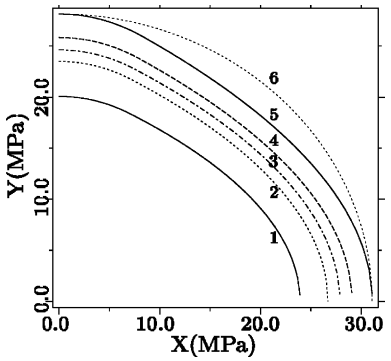

Fig. 5. Effective failure envelopes estimated by the different methods; dilute concentration of fibers (curve 1), the MEFM (5.15), (4.12) with the RDF (2.5) (curve 2); the MEFM (5.15), (4.12) with the RDF (2.4) (curve 3); the MEFM (5.15), (4.13) (curve 4); Mori–Tanaka approach (curve 5); elliptical approximation of Mori–Tanaka approach (curve 6).

approximation of the RDF (2.4). In general, interface failure occurs much more easily under a tensile normal than a compressive normal stress. That is, the normal strength $\sigma_n^{\max}$ is much greater for compression than for tension. As a result, interface failure under a compressive normal stress will not be considered in this paper. In Fig. 5 the failure envelopes are plotted in the first quadrant of a coordinates system $X = \langle \sigma_{11} \rangle \geqslant 0$ and $Y = \langle \sigma_{12} \rangle \geqslant 0$. The non elliptical curve 1 corresponds to the dilute concentration of fibers $c^{(1)} \ll 1$.

The curves 2 and 3 were estimated by the MEFM method (5.15), (4.12) with the RDF (2.5) and (2.4), respectively. Neglect of stress fluctuation (4.13) transforms the curve 3 into the curve 4. Ignoring of the binary interaction of fibers (3.9) automatically leads to the neglect of stress fluctuations (4.13) and tends to increase of the failure prediction as described by the curve 5. It should be mentioned that all curves 1–5 are not elliptical in the global coordinate system of macrostresses $\langle \boldsymbol{\sigma} \rangle$ (and, therefore, cannot be described by the quadratic Tsai and Wu, 1971 criterion) although the failure envelope (5.7) is described by a quadratic function of the traction $\langle \boldsymbol{\sigma}_{\mathbf{n}}^{-} \rangle_i$ in the local coordinate system connected with the fiber surface. The non elliptical shape of the effective failure envelope is demonstrated by the comparison of the curve 5 with the

elliptical curve 6 with the same semi-axes as the curve 5. It is interesting that the non elliptical shape of the effective limiting surface for the porous materials was demonstrated by Buryachenko (2001) in the related problem of onset of yielding at the porous surface.

The popular engineering simplification is based on the neglect of shearing failure in comparison with the failure initiated by the normal component of the traction $\boldsymbol{\sigma}_n^-$. That is equivalent to the assumption

$$\sigma_\tau^{\max} = \infty \tag{6.1}$$

the error of which we will estimate now by the example of the comparison of the curves 2 and 4 in Fig. 5 with the corresponding curves of effective failure envelopes plotted in the framework of the assumption (6.1). As can be seen in Fig. 6, the significant differences of effective failure envelopes estimated for the real failure parameters $\sigma_\tau^{\max}$ and $\sigma_n^{\max}$ as well as for the assumed one (6.1) are observed just at the small values σ_{11}. In the case of the well-stirred RDF (2.4) accompanied by the disregard of stress fluctuations in the fibers (4.13), the influence of the assumption (6.1) can be neglected in the area of moderate tension loading $\langle\sigma_{11}\rangle > 0.2\sigma_n^{\max}$.

The influence of the RDF on the effective failure envelopes will be estimated for the analytical representations (2.4) and (2.5) as well as for the numerical simulation by the CRM accompanied by the random shaking procedure. Only the perturbation method of estimations of the second moment of the interface stresses (4.11) by the MEFM and the failure criterion (5.15) will be analyzed. The difference between the estimations increasing with the rise of the fiber concentration vary from 1% till 6% at $c = 0.45$ and 0.75, respectively (see Fig. 7). In so doing the difference between the estimations obtained for the RDF (2.5) and for the simulated RDF does not exceed 0.8%.

Let us compare the effective failure envelopes predicted by the use of two different methods of the estimation of the second moments of interface stresses such as the perturbation method (4.11) and the method of the integral equations (4.15). In both cases the RDF simulated by the CRM accompanied by the random shaking procedure were used. As can be seen in Fig. 8, the maximum of the difference of the effective failure envelopes does not exceed 1.7% and is reached in the area of the large values of the tension components σ_{11} and the large fiber concentration. This difference of the effective failure envelopes insignificantly increases for an increasing elastic mismatch of the constituents. For, example the replacement of the real SCS-0 fibers by the model rigid fibers leads to the difference of the effective failure envelopes of 1.9% for $c = 0.75$ and $\langle\sigma_{12}\rangle = 0$.

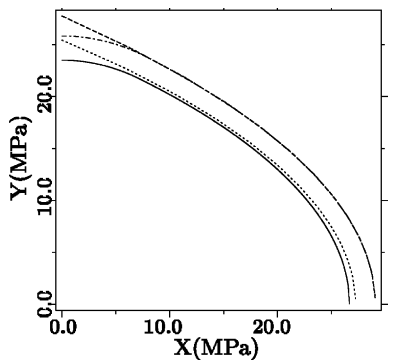

Fig. 6. Effect of shearing stresses on effective failure envelopes. Estimation by the MEFM (5.15), (5.13), (2.5) and (5.15), (5.14), (2.4) for the real failure parameters (solid and dot-dashed curves, respectively). Analogous estimations for the assumed failure parameter (6.1) (dotted and dashed curves, respectively).

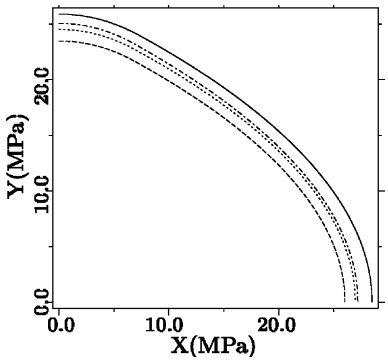

Fig. 7. Effective failure envelopes estimated for the different RDF: (2.4) ($c = 0.75$, solid curve), (2.5) ($c = 0.75$, dotted curve), CRM ($c = 0.75$ and 0.45, dot-dashed and dashed curves, respectively).

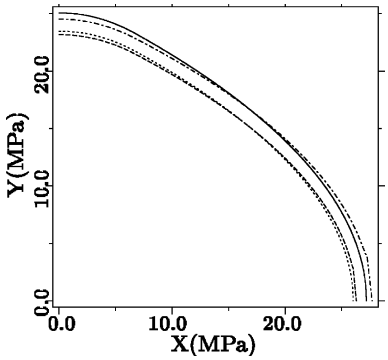

Fig. 8. Effective failure envelopes estimated by two different method of the evaluation of the second moment of stresses (real SCS-0 fibers): (4.11) ($c = 0.75$ and 0.45, solid and dotted curves, respectively), (4.15) ($c = 0.75$ and 0.45, dot-dashed and dashed curves, respectively).

7. Concluding remarks

A detailed discussion is given on the main hypotheses as well as the limitations of the proposed estimations and their possible generalizations. The main scheme as well as a brief discussion of limitations and of possible generalization and application of the methods proposed is presented.

Since the effective properties of fiber reinforced composites are dependent on the details of the microstructure, the quantitative description of the microtopology is crucial in the prediction of the overall mechanical and physical properties of these materials. In particular, micromechanical failure initiation in aligned fiber composites is sensitive to both local and non-local fiber distribution and many studies have shown that fracture properties of multi-phase composite materials are strongly affected by the spatial heterogeneity of the reinforcing phases. The MEFM has been used to accurately predict the effective properties of aligned fiber composite materials and to determine the dependence of the properties on the radial distribution function. The RDF of unidirectional composites was estimated by the use of several methods, including a numerical simulation exploring the collective rearrangement model with a random shaking procedure. The numerical simulation provided good agreement to RDF estimated from experimental data.

The estimation of the second moment of stresses including the second moment of fiber/matrix interface stresses was used in the proposed generalization of the tensor-polynomial strength criteria to the case of fiber/matrix interface failure taking into account the binary interaction inclusions effects, that are directly dependent on the fiber radial distribution function. This method allows one to take into account some nonlocal effects of micromechanical fiber/matrix interface failure prediction. The prediction of failure initiation envelopes for interface failure, obtained using several methods for representing the radial distribution function, are compared and found to vary considerably based on the manner in which the RDF is determined, on whether or not the fiber stress fluctuations are ignored, and on the binary interaction of the fibers. The non-elliptical shape of the effective failure envelops using the proposed method is demonstrated for the first quadrant $\sigma_{11} \geqslant 0$, $\sigma_{12} \geqslant 0$. The use of the developed effective failure envelopes for inhomogeneous microstructure can provide accurate material behavior predictions that can be realized through realistic representation of the constituent behavior and the realistic representation of the microtopology of the composites.

The progress in micromechanics of random structure composites is based on the methods of allowing for the statistical mechanics of a multi-particle system considering n-point correlation functions and direct multiparticle interaction of inhomogeneities. In so doing, the main disadvantage of the proposed method is the use of the hypothesis (H1), which is the basic hypothesis of of a number of popular methods of micromechanics (see for references Buryachenko, 2001). The use of this homogeneity hypothesis $\bar{\boldsymbol{\sigma}}_i(\mathbf{y} = \text{const.})$ $(\mathbf{y} \in v_i)$ (3.2) leads with necessity to the conclusion of the homogeneity of stress field inside ellipsoidal homogeneous inclusions according to the Eshelby theorem (3.4). However, micromechanical modeling and simulation of random structures are becoming more and more ambitious due to an advantage of modern computer software and hardware (see e.g. Buryachenko, in press). From one side, some models are developed with the aim to minimize the empirical elements and assumptions. In many cases, the detailing of basic microscopic phenomena leads to improvements of the accuracy, and provide the potential solution to the problems previously intractable. On the other side, there are ambitions to solve increasingly larger systems. Such methods, usually referred to the field of computational micromechanics, are based on the wide use of MC simulation with forthcoming numerical analysis for each random realization of multiparticle interactions of microinhomogeneities. At the present level of computer hardware and software they are only practical for realizations containing no more then a few thousands inhomogeneities; the effectiveness of MC method is questionable for the analysis of problems with an a priori unknown type of the effective constitutive equation such as e.g. the nonlocal problems for the functionally graded composites. In parallel with computational micromechanics mentioned above the classical or analytical micromechanics (such as e.g. presented method) are usually based on such fundamental notions as the Green function and Eshelby tensor. However, a combination of the general anisotropy of the matrix and the general shape of randomly located inclusions with continuously variable anisotropic properties presents an impenetrable barrier to the classical approaches using either analytical or numerical representation for the internal ($\mathbf{S}_i$) and external ($\mathbf{T}_i$) Eshelby tensors for inclusions. Because of this, the combining of opportunities of computational micromechanics with basic assumptions of analytical micromechanics is very promising. This makes possible the replacement of some analytical solutions for single and interacting inclusions by their numerical representations with forthcoming incorporation of results into the one from the general schemes of analytical micromechanics. The known numerical methods have a series of advantages and disadvantages, and it is crucial for the analyst to be aware of their range of applications. So, Buryachenko (2001) proposed to replace the approximate analytical solution of the binary interacted inclusions described by the matrix $\mathbf{Z}$ (3.8) by the first-order approximation of the solution obtained by the volume integral equation method (see for details Buryachenko and Pagano, in press). In the case of 2-D problems, Buryachenko and Kushch (in press) proposed the scheme of incorporation of a simple and powerful tool such as Kolosov–Muskhelishvili complex potentials method into the integral micromechanical equations of random structure composites.

The challenge of modern micromechanics is a development of the general method incorporating the solution for multiply interacting inhomogeneities obtained by highly accurate numerical methods into the most general scheme of analytical micromechanics.

Acknowledgements

This work was supported by the Air Force Research Laboratory, Materials and Manufacturing Directorate, Wright-Patterson AFB, OH, USA.

References

Arnould, J.F., 1982. Etude de l'endommagement des materiaux composites par decohesion fibre-matrice. In: Corvino, A. et al. (Eds.), Comptes Rendus des Troisiemes Journees Nationales sur les Composites (JNC-3). AMAS, Paris, 159–169.

Arsenault, R.J., Taya, M., 1987. Thermal residual stress in metal matrix composites. Acta Metall. 35, 651–659.

Benveniste, Y., 1987. A new approach to application of Mori–Tanaka's theory in composite materials. Mech. Mater. 6, 147–157.

Berryman, J.G., 1985. Measurement of spatial correlation functions using image processing techniques. J. Appl. Phys. 57, 2374–2384.

Bhattacharyya, A., Lagoudas, D.C., 2000. Effective elastic moduli of two-phase transversely isotropic composites with aligned clustered fibers. Acta Mech. 145, 65–93.

Bobeth, M., Diener, G., 1986. Field fluctuations in multicomponent mixtures. J. Mech. Phys. Solids 34, 1–17.

Buryachenko, V.A., 2001. Multiparticle effective field and related methods in micromechanics of composite materials. Appl. Mech. Rev. 54, 1–47.

Buryachenko, V.A., in press. Editorial of the Special Issue Entitled Recent Advances in Micromechanics of Composite Materials. Int. J. Multiscale Comput. Eng. 2.

Buryachenko, V.A., Kushch, V.I., in press. Effective transverse elastic moduli of composites at non-dilute concentration of a random field of aligned fibers. ZAMP.

Buryachenko, V.A., Pagano, N.J., 2003. Nonlocal models of stress concentrations and effective thermoelastic properties of random structure composites. Math. Mech. Solids 8, 403–433.

Buryachenko, V.A., Pagano, N.J., in press. Multiscale analysis of multiple interacting inclusions problem: Finite number of interacting inclusions. Math. Mech. Solids 9.

Buryachenko, V.A., Pagano, N.J., Kim, R.Y., Spowart, J.E., 2003. Quantitative description of random microstructures of composites and their effective elastic moduli. Int. J. Solids Struct. 40, 47–72.

Buryachenko, V.A., Rammerstorfer, F.G., 1998. Thermoelastic stress fluctuations in random structure coated particulate composites. European J. Mech. A/Solids 17, 763–788.

Buryachenko, V.A., Tandon, G.P., in press. Estimation of effective elastic properties of random structure composites for arbitrary inclusion shape and anisotropy of components using finite element analysis. Int. J. Multiscale Comput. Eng. 2.

Christensen, R.M., 1979. Mechanics of Composite Materials. Wiley Interscience, NY.

Desrumaux, F., Meraghni, F., Benzeggagh, M.L., 2001. Generalized Mori–Tanaka scheme ti model anisotropic damage using numerical Eshelby tensor. J. Compos. Materials 35, 603–623.

Ghassemieh, E., Nassehi, V., 2001. Prediction of failure and fracture mechanisms of polymeric composites using finite element analysis. Part 2 Fibre reinforced composites. Polym. Composites 22, 542–554.

Ghosh, S., Mukhopadhyay, S.N., 1991. A two-dimensional automatic mesh generator for finite element analysis for random composites. Compos. Struct. 41, 245–256.

Ghosh, S., Nowak, Z., Lee, K., 1997. Quantitative characterization and modeling of composite microstructures by Voronoi cells. Acta Mater. 45, 2215–2234.

Green, P.I., Sibson, R., 1977. Computing Dirichlet tesselations in the plane. Computer J. 21, 168–173.

Hansen, J.P., McDonald, I.R., 1986. Theory of Simple Liquids. Academic Press, NY.

Kanaun, S.K., Levin, V.M., 1994. Effective field method in mechanics of matrix composite materials. In: Markov, K.Z. (Ed.), Advances in Mathematical Modeling of Composite Materials. World Scientific, Singapore, New Jersey, pp. 1–58.

Kreher, W., Pompe, W., 1989. Internal Stresses in Heterogeneous Solids. Akademie-Verlag, Berlin.

Kröner, E., 1958. Berechnung der elastischen Konstanten des Vielkristalls aus den Konstanstanten des Einkristalls. Z. Physik. 151, 504–518.

Kutlu, Z., Chang, F.K., 1995. Composite panels containing multiple through-the-width delaminations and subjected to compression. Part I: Analysis. Compos. Struct. 31, 273–296.

Kwon, Y.W., Eren, H., 2000. Micromechanical study of interface stresses and failure in fibrous composites using boundary element method. Polym. Polym. Compos. 8, 369–386.
Lax, M., 1952. Multiple scattering of waves II. The effective fields dense systems. Phys. Rev. 85, 621–629.
Lee, J.A., Mykkanen, D.L., 1987. Metal and Polymer Matrix Composites. Noyes Data Corporation, NY.
Lipton, R., 2003. Assessment of the local stress state through macroscopic variables. Phil. Trans. R. Soc. Lond. 361, 921–946.
Meraghni, F., Blaman, C.J., Benzeggagh, M.L., 1996. Effect of interfacial decohesion on stiffness reduction in a random discontinuous-fibre composite containing matrix microcracks. Compos. Sci. Technol. 56, 541–555.
Milton, G.W., 2003. The theory of composites. In: Applied Computation Mathematics, vol. 6. Cambridge University Press.
Mori, T., Tanaka, K., 1973. Average stress in matrix and average elastic energy of materials with misfitting inclusions. Acta Metall. 21, 571–574.
Mura, T., 1987. Micromechanics of Defects in Solids. Martinus Nijhoff, Dordrecht.
Mura, T., Shodia, H.M., Hirose, Y., 1996. Inclusion problems. Appl. Mech. Rev. 49 (2), S118–S127.
Nemat-Nasser, S., Hori, M., 1993. Micromechanics: Overall Properties of Heterogeneous Materials. Elsevier, North-Holland.
Ponte Castañeda, P., Suquet, P., 1998. Nonlinear composites. Adv. Appl. Mech. 34, 171–302.
Pyrz, R., Bochenek, B., 1998. Topological disorder of microstructure and its relation to the stress field. Int. J. Solids Struct. 35, 2413–2427.
Reddy, J.N. (Ed.), 1994. Mechanics of Composite Materials. Selected works of N.J. Pagano. Kluwer Academic Publishers, Dordrecht, NY.
Reifsnider, K.L., Gao, Z., 1991. A micromechanics models for composites under fatigue loading. Int. J. Fatigue 13, 149–156.
Shermergor, T.D., 1977. The Theory of Elasticity of Microinhomogeneous Media. Nauka, Moscow (in Russian).
Sun, C.T., Zhou, S.G., 1988. Failure of quasi-isotropic composite laminates with free edges. J. Reinf. Plast. Comp. 7, 515.
Tandon, G.P., Kim, R.Y., Bechel, V.T., in press. Construction of the fiber-matrix interfacial failure in a polymer matrix composites. Int J. Multiscale Comput. Eng. 2.
Theocaris, P.S., 1991. The elliptic paraboloidal failure criterion for cellular solids and brittle forms. Acta Mech. 89, 93–121.
Torquato, S., 2002a. Random Heterogeneous Materials: Microstucture and Macroscopic Properties. Springer-Verlag.
Torquato, S., 2002b. Statistical description of microstructures. Annu. Rev. Mater. Res. 32, 77–111.
Torquato, S., Lado, F., 1992. Improved bounds on the effective elastic moduli of random arrays of cylinders. ASME. J. Appl. Mech. 59, 1–6.
Tsai, S.W., Wu, E.M., 1971. A general theory of strength for anisotropic materials. J. Comp. Mater. 5, 58–80.
Willis, J.R., 1981. Variational and related methods for the overall properties of composites. Advances in Applied Mechanics 21, 1–78.
Zhiging, J., Tennysin, R.C., 1989. Closure of cubic tensor polynomial failure surface. J. Comp. Mech. 23, 208–231.